*mining*

MDPI

*Article*

# Archival Mine-Plan Reconstruction and GIS-Based Interpretation of Spatially Variable 2007–2026 Surface Elevation Change in the Petroșani Coal Basin, Romania

**Teodora Gavrilescu [1,*] and Vlad Păunescu [2]**

[1] Faculty of Geology and Geophysics, Doctoral School of Geology, University of Bucharest, 020956 Bucharest, Romania
[2] Department of Mathematics, Physics and Land Measurements, Faculty of Land Reclamation and Environmental Engineering, University of Agronomic Sciences and Veterinary Medicine of Bucharest, 011464 Bucharest, Romania; vlad.paunescu@topoexim.ro
* Correspondence: teodora.gavrilescu@s.unibuc.ro

**Abstract**

Historical underground workings in the Maleia–Livezeni sector of the Petroșani Coal Basin were reconstructed from four archival mining plans and a coordinate-referenced Drawing Exchange Format (DXF) dataset. Twelve extraction-sector polygons, principal galleries, exploitation limits, dated mining stages, and 567 internally checked mining-elevation annotations associated with Coal Seam No. 3 were integrated in a geographic information system (GIS) using the Romanian Stereo 70 coordinate reference system (EPSG:3844). Net elevation differences between 2007 and 2026 at seventeen surface benchmarks were used as response variables. Nearest-feature relationships and mining-exposure indicators for 50, 100, and 150 m neighbourhoods were evaluated using exploratory Spearman rank correlations. Among the originally selected 50, 100, and 150 m neighbourhoods, cumulative gallery length within 50 m showed the strongest planimetric association with $|\Delta_Z|$ ($\rho = 0.734$, $p = 0.0008$, q = 0.010), while extraction-sector coverage and gallery length remained positively associated at broader scales. R19 showed the greatest immediate extraction-sector exposure, whereas R14, which recorded the largest elevation loss, was characterised by a broader concentration of surrounding workings. R09 recorded the smallest elevation change and was approximately 470 m from the nearest reconstructed extraction sector. Cumulative mining configuration was more informative than nearest-sector distance alone for interpreting spatially variable net surface-elevation change in this legacy mining setting and highlighted the limitations of archival GIS reconstruction.

**Keywords:** surface elevation change; historical mine plans; GIS reconstruction; underground coal mining; Petroșani Coal Basin

Check for updates

Academic Editor: Claudio Oggeri

Received: 10 August 2026
Revised: 31 August 2026
Accepted: 5 September 2026
Published: 8 September 2026

**Copyright:** © 2026 by the authors. Licensee MDPI, Basel, Switzerland. This article is an open access article distributed under the terms and conditions of the Creative Commons Attribution (CC BY) license.

## 1. Introduction

Underground coal extraction modifies the initial stress field and may produce surface deformation both during mining and after mine closure. The magnitude and spatial distribution of this deformation depend on interacting factors such as extraction geometry and chronology, mining depth, seam thickness, overburden behaviour, and structural discontinuities [1–7]. Although geodetic monitoring, remote sensing, analytical methods, and numerical modelling can quantify ground movement [8–11], deformation measurements alone do not always explain why neighbouring surface locations exhibit different responses.

Historical mining documentation provides valuable spatial and temporal evidence for interpreting legacy underground workings. Archived plans may preserve extraction-sector boundaries, galleries, exploitation limits, pillars, mining elevations, and successive mining stages. After coordinate verification and structured digitisation within a geographic information system (GIS), these records can be integrated with present-day surface observations to reconstruct historical mining configurations [12]. However, because archival plans may contain positional inconsistencies or incomplete operational information, reconstructed geometries must be treated as plan-based spatial estimates and interpreted with explicit consideration of uncertainty [13].

Previous studies have generally addressed deformation monitoring and historical mine reconstruction as related but distinct tasks. Geodetic, InSAR, analytical, and modelling studies have primarily focused on quantifying surface deformation [8–11], whereas GIS-based investigations of legacy mine information have emphasized georeferencing, inventory, and spatial reconstruction of historical workings [12,13]. The present study links these two strands by transforming heterogeneous archival mine-plan information into benchmark-specific, multi-scale exposure indicators and by integrating mining-elevation annotations with independently observed surface-elevation changes. This framework enables a direct spatial comparison between cumulative underground mining configuration and heterogeneous benchmark response while explicitly retaining the uncertainties inherent in archival reconstruction.

This approach is particularly relevant in long-established mining districts, where several adjacent panels were exploited successively. In such settings, the present deformation pattern may reflect the cumulative configuration of multiple workings rather than the effect of one isolated panel. Nearest-feature distance alone may therefore provide an incomplete representation of mining influence, whereas multi-scale indicators describing extraction-sector coverage, gallery concentration, and the number of surrounding mining sectors may better characterize the historical underground context.

The Petroșani Coal Basin in the Southern Carpathians of Romania provides a suitable case study because of its lithological heterogeneity, tectonic compartmentalization, and complex history of underground coal exploitation. Within the Maleia–Livezeni sector, Coal Seam No. 3 was mined through several neighbouring panels, galleries, inclined workings, and submining sectors, mainly during the first decade of the twenty-first century. The successive development of these workings created a spatially complex mining configuration that can be compared with the cumulative elevation differences recorded at surface benchmarks.

Previous investigations in the Jiu Valley have addressed complementary aspects of mining-induced ground deformation and its geological context. Global Positioning System (GPS) monitoring in the Petroșani coal-mining area documented spatially variable surface subsidence and demonstrated that deformation was not uniformly distributed across the mining basin [14]. The Research of Excellence Programme (CEEX) combined geological, mining, geodetic, and deformation-monitoring information to investigate land affected by underground exploitation in the Petroșani Basin [15], while geological studies have characterized the lithological and coal-bearing succession of the Jiu Valley and its pronounced spatial heterogeneity [16]. More recent GNSS observations confirmed persistent and spatially variable benchmark-level elevation losses over the 2007–2026 interval [17]. Together, these studies demonstrate that surface response in the Jiu Valley is spatially heterogeneous and must be interpreted in relation to both mining configuration and geological setting. However, they did not reconstruct the specific Maleia–Livezeni archival mine-plan geometry into benchmark-level multi-scale exposure indicators, which is the focus of the present study.

Previous GPS monitoring in the Petroșani mining area also documented spatially variable horizontal and vertical surface motions, with the largest movements occurring in the older central mining sector [14].

In this study, four archival mining plans and a coordinate-referenced Drawing Exchange Format (DXF) dataset were used to reconstruct twelve extraction sectors, principal galleries, exploitation limits, documented mining stages, and mining-elevation annotations. Cumulative 2007–2026 elevation differences measured at seventeen benchmarks were used as response values. The analysis combined nearest-feature relationships with mining-exposure indicators calculated within 50, 100, and 150 m neighbourhoods and within a 100–150 m annulus.

The objectives were to (1) reconstruct the documented spatial configuration and chronology of underground exploitation in Coal Seam No. 3; (2) quantify the position of the monitoring benchmarks relative to extraction sectors and principal galleries; and (3) evaluate whether spatially variable elevation loss is more consistently associated with cumulative mining exposure than with nearest-feature distance alone. Geological information was used as an interpretative framework, while the independent effects of lithology, faults, groundwater, overburden thickness, and rock-mechanical properties were not quantified at benchmark scale.

## 2. Geological and Mining Context

### *2.1. Regional Geological Framework*

The Petroșani (Jiu Valley) Coal Basin is an Oligocene intramontane coal-bearing basin located in the Southern Carpathians of Romania [15,16]. It is approximately 45 km long, 1.5–9 km wide, and 163 km$^2$ in area [15]. It lies near the contact between the Getic domain and the Danubian Autochthon, and its coal-bearing succession is divided into mining blocks by longitudinal and transverse faults.

The basin fill comprises a lower conglomeratic complex, a 300–600 m thick productive marl–clay complex containing the principal coal horizons, and an upper detrital complex dominated by conglomerates and sandstones [15]. Alternation between competent sandstone or conglomeratic beds and weaker claystone, marl, and carbonaceous-shale intervals creates pronounced lithological and mechanical heterogeneity.

This heterogeneity and the tectonic compartmentalization provide the geological framework for interpreting spatially variable surface elevation change in the post-mining setting. Their effects could not, however, be quantified at individual benchmarks.

### *2.2. Coal-Bearing Succession and Coal Seam No. 3*

Coal Seam No. 3, the most productive coal bed of the Oligocene Dâlja–Uricani Formation, is the principal seam represented in the analysed plans (Figure 1) [15,16]. It may contain one to thirty coal benches separated by clay-rich or sterile intercalations; the upper part is comparatively compact, whereas sterile interbeds generally increase toward the floor. The roof comprises alternating sandstones and clay-rich rocks, while the floor is dominated by hard siliceous or quartzitic sandstones and sandy claystones [15].

Within Block VIA, documented seam thickness ranges from approximately 2 to 16.8 m, with a locally exploitable thickness of about 10–10.5 m [15]. The contrast between competent sandstone beds and weaker fine-grained units provides a plausible framework for differential roof collapse, stress redistribution, and delayed compaction, although these processes were not measured beneath individual benchmarks.

### *2.3. Geological and Mining Setting of the Maleia–Livezeni Sector*

The study area covers historical workings in Blocks VI, VIA, and VII of the Maleia–Livezeni sector. The Livezeni deposit is tectonically compartmentalized, and seam dips decrease from approximately 15–20° on the northern flank to 8–10° southward [15]. Coal Seam No. 3 was exploited at depths reaching about 300 m using mechanized longwall methods, extraction in slices, and total roof caving [15].

A conceptual representation of the documented exploitation method is shown in Figure 1. The schematic illustrates mechanized longwall extraction in slices with total roof caving and the associated overburden disturbance. It is intended only to support interpretation of the mining context and does not represent a scaled three-dimensional reconstruction of the actual Maleia–Livezeni workings.

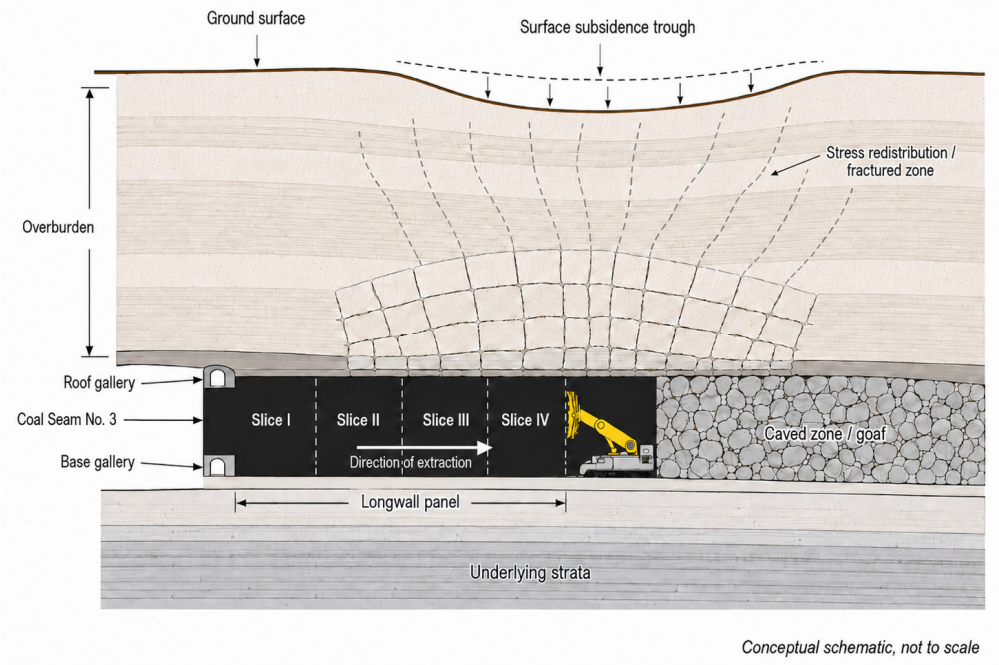



**Figure 1.** Conceptual schematic of mechanized longwall extraction in slices with total roof caving in Coal Seam No. 3. The diagram illustrates the longwall panel, roof and base galleries, caved zone (goaf), overburden disturbance, stress redistribution/fracturing, and the conceptual development of a surface subsidence trough. The schematic is not to scale and does not represent the exact three-dimensional geometry of the Maleia–Livezeni underground workings.

The archival documentation records extraction sectors, exploitation limits, base and roof galleries, directional workings, ventilation and collector inclines, access routes, pillars, and dated mining stages. The reconstructed sectors include Panel 3 North, Panel 1 North, Panel 2 North submining, Panel 4 submining, and neighbouring extraction areas, developed mainly between 2000 and 2007.

Variable seam inclination, substantial extracted thickness, roof caving, tectonic compartmentalization, and contrasting roof lithologies provide an interpretative framework. Benchmark-specific borehole, fault, groundwater, and rock-mechanical data were unavailable, so geological controls were not tested quantitatively.

## 3. Data and Methods

### *3.1. Data Sources and Research Design*

The study integrated four archival underground mining plans, a coordinate-referenced DXF compilation, geological and mining information from the CEEX project (Contract No.

722/2006) [15], and net 2007–2026 elevation differences previously published for seventeen benchmarks [17].

The archival sources documented extraction-sector boundaries, exploitation limits, principal galleries, pillars, mining elevations, production information, and dated mining stages in Coal Seam No. 3, Blocks VI, VIA, and VII. Because their detail and spatial coverage varied, they were treated as historical cartographic evidence rather than as a survey-grade three-dimensional mine model.

The published Global Navigation Satellite System (GNSS) values were used only as response variables and were not reprocessed. The new contribution consists of the GIS reconstruction, chronology, multi-scale exposure indicators, internally checked mining-elevation annotations, and exploratory statistical comparison with the benchmark elevation losses.

The previously published study [17] focused on the GNSS monitoring design, observation processing, measurement uncertainty, and the magnitude of the 2007–2026 benchmark displacements. The present manuscript does not repeat or reanalyse those geodetic procedures. The published net elevation differences are used exclusively as response variables for a new archival mine-plan reconstruction, mining-chronology assessment, multi-scale GIS exposure analysis, and internally checked mining-elevation annotations. The extraction-sector polygons, gallery-exposure metrics, reconstructed chronology, and statistical comparisons reported here were not included in the previous study.

### *3.2. GIS Reconstruction and Quality Control*

The DXF compilation was imported into the open-source geographic information system QGIS [18] and processed in the Romanian Stereo 70 coordinate reference system (EPSG:3844). Benchmark geometries were created using the standard GIS order Point (Easting, Northing), accounting for the Romanian surveying convention X = northing and Y = easting.

Relevant gallery walls, extraction limits, dates, and technical annotations were retained. Principal galleries were digitised as centre lines, and closed polylines representing extracted or submined areas were converted into twelve extraction-sector polygons. Attributes were assigned only when supported by explicit labels or clear spatial relationships; ambiguous features were excluded from quantitative analysis.

Quality control included comparison with the source DXF, inspection of line continuity and attributes, and GEOS validity testing. All twelve retained polygons were valid. Because no independent underground control dataset was available, reconstructed positions and benchmark-to-feature distances are interpreted as plan-based estimates rather than centimetre-level locations.

Distances were computed from the reconstructed plan geometries and are reported as approximate GIS-derived values. Their numerical precision does not imply survey-grade positional accuracy.

### *3.3. Reconstruction of the Documented Mining Chronology*

Chronology was reconstructed from dated annotations, extraction-front positions, production labels, and mining stages. Dates were assigned to a sector only when their graphical relationship was clear; ambiguous dates were retained as documentary information but excluded from formal interpretation.

The best-documented activity occurred between 2000 and 2007. Panel 3 North contained explicit stages for 2000–2002, Panel 2 North submining was documented approximately between 2002 and 2007, and Panel 4 submining was documented mainly after 2003. Panel 1 North was placed earlier in the sequence, but no precise interval could be assigned.

The chronology was interpreted at annual and panel scales and represents a documented sequence, not a complete production history or a precise temporal predictor of the 2007–2026 elevation changes.

### *3.4. Integration of Benchmark Elevation Differences*

The response dataset comprised net elevation differences between the 2007 and 2026 surveys at seventeen benchmarks. Negative values indicate elevation loss, while $|\Delta_Z|$ was used in statistical analysis so that larger downward changes corresponded to larger positive magnitudes.

Coordinates and elevation differences were taken from the previously published GNSS study [17]; the field observations, processing, adjustment, and uncertainty analysis were not repeated. All seventeen benchmarks were included in the planimetric analysis. R14, R19, R07, R06, and R09 were selected only for illustrative comparison and were not excluded from the full statistical dataset.

Because only two observation epochs were available, the values represent net change over nineteen years and do not establish whether deformation was continuous, episodic, or characterised by a constant rate.

Accordingly, throughout the statistical analysis, $\Delta_Z$ is interpreted strictly as a net elevation difference between the two observation epochs and not as a time-resolved subsidence history.

### *3.5. Planimetric Mining-Exposure Analysis*

Planimetric relationships were evaluated through polygon containment, nearest-feature analysis, and circular neighbourhoods. For each benchmark, QGIS was used to determine whether it lay inside an extraction sector, the nearest extraction sector and principal gallery, and their planimetric distances. A sector distance of 0 m denotes polygon containment, not distance to a boundary or underground void.

Buffers of 50, 100, and 150 m were intersected separately with extraction-sector polygons and gallery centre lines. For each radius, the analysis calculated extraction-sector area and percentage coverage, cumulative gallery length, and the number of distinct extraction sectors. Each sector was counted once using its unique identifier. A 100–150 m annulus was analysed separately to distinguish immediate from peripheral exposure; non-intersections were assigned zero.

To assess whether the relationship between cumulative principal-gallery length and the magnitude of the net elevation change was sensitive to the selected neighbourhood radii, an additional radius-sensitivity analysis was performed using 25, 50, 75, 100, 125, and 150 m circular neighbourhoods.

Buffers were processed independently for each benchmark and could overlap. The selected radii are comparative GIS scales, not mechanically calibrated influence zones, legal hazard limits, or geotechnical safety boundaries.

The 50, 100, and 150 m radii were selected as nested comparative scales representing the immediate, intermediate, and broader local mining context, considering benchmark spacing and the mapped density of the reconstructed workings. They were not derived from a calibrated subsidence or influence-angle model.

For each radius, cumulative principal-gallery length was recalculated for all seventeen benchmarks and compared with $|\Delta_Z|$ using Spearman rank correlation. These additional radii were used solely as a robustness check and were not interpreted as calibrated mining-influence distances.

### *3.6. Mining-Elevation Data Extraction and Internal Consistency Check*

Numeric DXF text values between 200 and 800 m were converted to points to provide an exploratory vertical context. An annotation was retained when its numeric text

value agreed with the Z coordinate of the corresponding three-dimensional DXF geometry within 0.01 m. Because both values originated from the same DXF dataset, this procedure represents an internal consistency check rather than independent validation. A total of 567 internally checked mining-elevation annotations met this criterion.

Because the points represented galleries, inclined workings, collectors, extraction sectors, and other technical features, they were not interpreted as exact panel depths or as a complete three-dimensional mine model. Within 150 m of each benchmark, the number, minimum, maximum, mean, median, range, and standard deviation of internally checked mining elevations were calculated, together with approximate vertical separations from the 2007 surface elevation.

Statistical analysis was restricted to ten benchmarks with at least ten internally checked mining-elevation points. R18, with one value, was retained only descriptively; benchmarks without supported vertical information remained in the planimetric analysis. Unequal point density and feature type were treated as important limitations.

### *3.7. Exploratory Statistical Analysis*

Spearman rank correlations were used to compare $|\Delta_Z|$ with the planimetric indicators for all seventeen benchmarks and with mining-elevation indicators for the ten benchmarks having sufficient vertical data. This non-parametric method was selected because of the small sample, non-normal and zero-inflated variables, and the absence of an assumed linear relationship.

All tests were two-sided with an initial threshold of $p < 0.05$. Benjamini–Hochberg false-discovery-rate-adjusted q values were reported for multiple comparisons [19]. Calculations were performed in Python 3.13.5 using SciPy 1.17.0 [20].

The Python script used to reproduce the reported Spearman correlations, multiple-testing adjustments, and sensitivity analyses is provided as Supplementary File S1.

The complete benchmark-level dataset used in the planimetric and vertical analyses is provided in Supplementary Table S1.

The benchmark-level cumulative principal-gallery lengths used in the radius-sensitivity analysis are provided in Supplementary Table S2.

The coefficients were interpreted as exploratory associations, not causal or predictive relationships, because the benchmarks were spatially clustered, buffers could overlap, variables at different radii were correlated, and only two monitoring epochs were available. Documentary evidence, GIS-derived relationships, and geological interpretation were kept distinct throughout the analysis. The complete analytical workflow, from archival data preparation to statistical and geological interpretation, is summarised in Figure 2.

Because the small and spatially clustered benchmark network did not support a robust spatial-autocorrelation model, the reported $p$ and q values are used only for exploratory screening and not for confirmatory inference.

Because the standard deviation of documented mining elevations showed the strongest association in the vertical subset, an additional leave-one-benchmark-out sensitivity analysis was performed for this relationship. Spearman's ρ was recalculated ten times, each time excluding one of the ten benchmarks with supported vertical information.

To assess whether the strongest planimetric association was driven by an individual observation, a leave-one-benchmark-out sensitivity analysis was performed.

As an additional robustness assessment for the strongest planimetric association, non-parametric resampling was performed for cumulative gallery length within 50 m. A paired bootstrap with 10,000 benchmark resamples was used to estimate a percentile-based 95% confidence interval for Spearman's ρ. In addition, a two-sided Monte Carlo permutation test with 100,000 random permutations of the response values was performed. These

resampling analyses were used as sensitivity checks and do not remove the limitations associated with spatial clustering or overlapping benchmark neighbourhoods.

The methodological workflow adopted in this study is summarized in Figure 2.

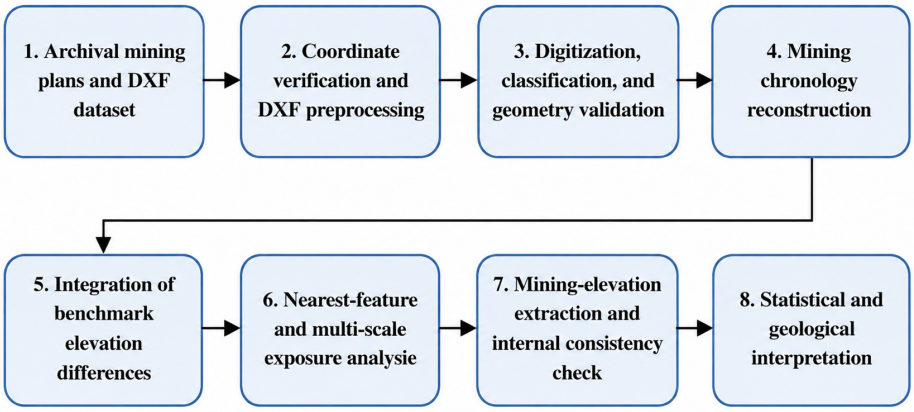



**Figure 2.** Methodological workflow used to reconstruct the historical underground workings and evaluate their spatial relationships with cumulative benchmark elevation differences.

## 4. Results

### *4.1. Reconstructed Underground-Working Configuration*

The GIS reconstruction produced twelve valid extraction-sector polygons, a connected network of principal galleries, exploitation limits, and the positions of the seventeen surface benchmarks relative to the reconstructed workings in Coal Seam No. 3, Blocks VI, VIA, and VII. The mapped sectors included Panel 1 North, Panel 2 North submining, Panel 3 North, Panel 4 submining, and neighbouring areas. Base, roof, directional, access, ventilation, collector, inclined, and connecting galleries formed an interconnected system rather than isolated workings. Panel 3 North was explicitly documented in Coal Seam No. 3, Slice I, Block VI, with a reported production of 68,800 tonnes.

Differences in sector size, adjacency, and gallery connections placed benchmarks inside sectors, near their margins, among several workings, or outside the main reconstructed mining concentration.

The reconstructed spatial distribution of the extraction sectors, principal galleries, and monitoring benchmarks is shown in Figure 3.

### *4.2. Documented Mining Chronology*

The archival documentation recorded successive extraction and infrastructure-development stages, most consistently between 2000 and 2007. Panel 3 North contained explicit stages for 2000–2002; Panel 2 North submining was documented approximately between 2002 and 2007; and Panel 4 submining was documented mainly after 2003. Panel 1 North belonged to the earlier sequence, but its precise interval was unavailable.

The sequence indicates that adjacent sectors and galleries were developed successively rather than simultaneously. However, the plans lack uniform monthly records, extraction rates, and complete opening or closure dates, so Table 1 represents a plan-based chronology rather than a complete production history.

Because surface observations are available only for 2007 and 2026, the reconstructed mining chronology cannot be temporally matched to the observed elevation changes. The available data do not establish whether the net 2007–2026 elevation differences developed predominantly soon after the documented mining stages, accumulated gradually over the nineteen-year interval, or resulted partly from later episodic movements. The chronology

is therefore used only to characterize the cumulative historical mining configuration and not to infer the timing or rate of surface deformation.

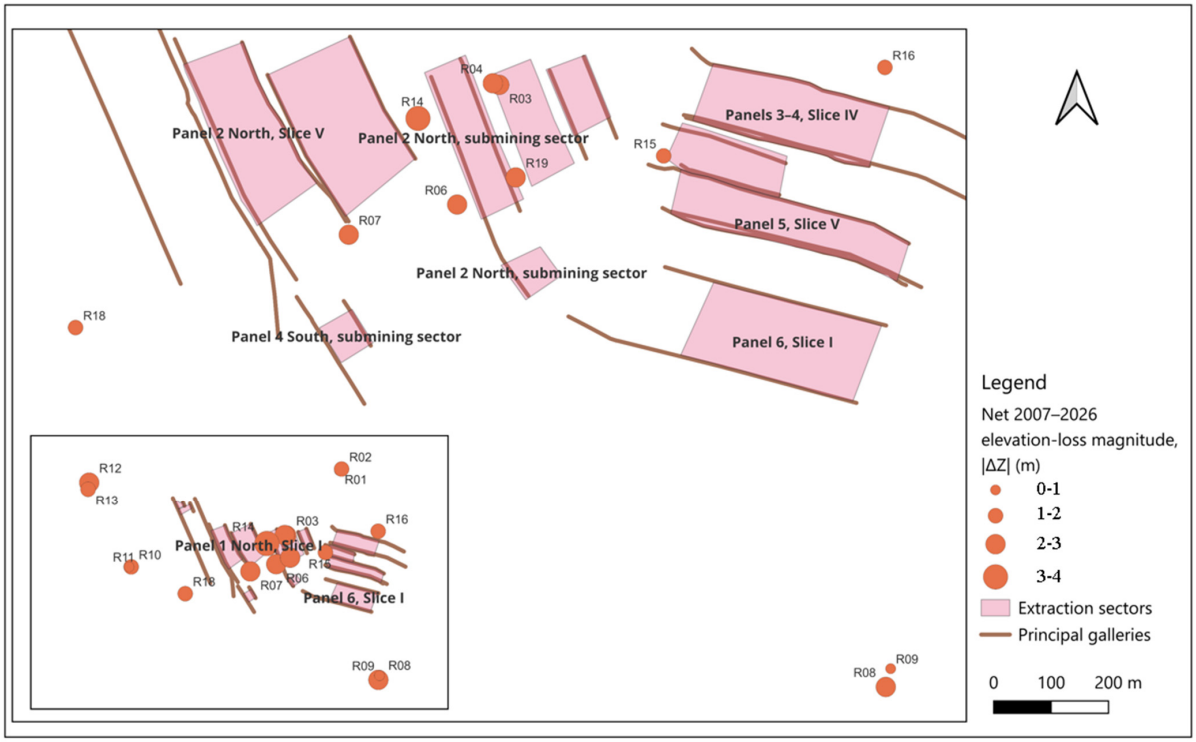



**Figure 3.** GIS reconstruction of the historical underground workings and benchmark-level net surface-elevation changes in the Maleia–Livezeni sector. The main map shows reconstructed extraction sectors, principal-gallery centre lines, and surface benchmarks, with benchmark symbols scaled according to the magnitude of the net 2007–2026 elevation loss, $|\Delta_Z|$. The inset presents the complete seventeen-benchmark monitoring network. The underground geometry was reconstructed from archival mining plans and a coordinate-referenced DXF compilation in the Romanian Stereo 70 coordinate reference system (EPSG:3844). The benchmark symbols represent point observations and should not be interpreted as a continuous subsidence surface. Feature positions are plan-based spatial estimates.

**Table 1.** Mining sectors and chronological information reconstructed from the archival documentation. The intervals represent explicitly documented or approximately inferred plan-based activity periods rather than a complete operational history.

| Coal Seam and Mining Block | Mining Sector | Documentary Evidence | Documented Interval | Principal Mapped Elements |
|---|---|---|---|---|
| Coal Seam No. 3, Slice I, Block VI | Panel 3 North | Panel label, production annotation, and explicitly dated mining stages | 2000–2002; explicitly documented stages | Base, roof, and directional galleries; extraction limits |
| Coal Seam No. 3, Block VI | Panel 1 North | Panel label and spatial relationship with earlier documented workings | Earlier part of the reconstructed sequence; precise interval unavailable | Extraction limits and associated galleries |
| Coal Seam No. 3, Block VI | Panel 2 North submining | Dated extraction and infrastructure annotations | Approximately 2002–2007 | Base and roof galleries; ventilation and collector workings |
| Coal Seam No. 3, Blocks VI–VIA | Panel 4 submining | Panel label and dated mining stages associated with adjoining workings | Mainly after 2003 | Sector limits; access, ventilation, inclined, and collector workings |

### *4.3. Benchmark Response and Nearest-Feature Relationships*

Net elevation loss varied from −0.082 m at R09 to −3.853 m at R14. R19, R07, and R06 also recorded large losses of −2.876, −2.860, and −2.848 m, respectively.

For visual comparison with the reconstructed underground workings, the benchmark symbols in Figure 3 were scaled according to the magnitude of the net 2007–2026 elevation loss.

This representation shows the observed benchmark-level changes relative to the 2007 reference epoch without implying a continuous deformation surface between monitoring points.

These four high-magnitude benchmarks were close to mapped sectors and galleries: nearest-sector distances ranged from 2.34 m at R19 to 39.08 m at R14, and nearest-gallery distances from 14.86 to 41.82 m. In contrast, R09 was approximately 470 m from the nearest reconstructed sector and 466 m from the nearest gallery, consistent with its peripheral location.

R12 represents an important contrasting observation. It recorded a net elevation difference of −2.556 m despite being located more than 600 m from the reconstructed mining features and outside the analysed 150 m mining-exposure neighbourhoods. This configuration cannot be explained by the reconstructed mine geometry used in the present study. Possible explanations include incomplete archival coverage or undocumented workings, broader-scale ground deformation, local geological or hydrogeological conditions, benchmark disturbance, or other non-mining influences. Because none of these alternatives can be distinguished with the available dataset, R12 was retained in the statistical analysis without assigning a specific cause to its observed elevation change. R03 and R04 lay inside sector polygons and therefore had sector distances of 0 m. Overall, proximity was informative but insufficient as a stand-alone explanation (Table 2).

**Table 2.** Net 2007–2026 elevation differences and nearest-feature relationships for five representative benchmarks. Negative $\Delta_Z$ values indicate elevation loss.

| Benchmark | $\Delta_Z$ (m) | Position Relative to Mapped Extraction Sectors | Distance to Nearest Extraction Sector (m) | Distance to Nearest Principal Gallery (m) |
|---|---|---|---|---|
| R14 | −3.853 | Outside | 39.08 | 41.82 |
| R19 | −2.876 | Outside; immediately adjacent | 2.34 | 14.86 |
| R07 | −2.860 | Outside | 32.52 | 23.17 |
| R06 | −2.848 | Outside | 29.97 | 36.91 |
| R09 | −0.082 | Outside; peripheral to reconstructed workings | 470.03 | 466.16 |

### *4.4. Multi-Scale Mining-Exposure Patterns*

Eight benchmarks intersected at least one extraction sector within 150 m. R19 showed the greatest immediate coverage within 50 m (65.20%), whereas R14 combined limited 50 m coverage (9.78%) with high 150 m coverage (48.32%) and the highest 100–150 m annular coverage (49.50%).

Gallery concentration showed a different ranking. R15 had the greatest cumulative gallery length within 150 m (953.35 m), followed by R14 (786.60 m), yet R15 did not record the greatest elevation loss. R06, R15, and R19 each intersected four distinct sectors within 150 m, while R14 and R07 intersected three.

Thus, high losses occurred under different configurations: strong immediate exposure at R19, broad peripheral exposure at R14, and mixed sector–gallery settings at R06 and R07. No single exposure indicator reproduced the complete benchmark ranking (Table 3).

**Table 3.** Multi-scale mining-exposure indicators for benchmarks intersecting at least one reconstructed extraction sector within 150 m. Negative $\Delta_Z$ values indicate elevation loss.

| Benchmark | $\Delta_Z$ (m) | Coverage Within 50 m (%) | Coverage Within 150 m (%) | Coverage in 100–150 m Annulus (%) | Gallery Length Within 150 m (m) | Distinct Sectors within 150 m |
|---|---|---|---|---|---|---|
| R03 | −2.067 | 54.94 | 46.94 | 40.50 | 479.54 | 3 |
| R04 | −2.458 | 51.67 | 43.79 | 34.71 | 463.16 | 3 |
| R06 | −2.848 | 14.26 | 25.05 | 26.22 | 537.14 | 4 |
| R07 | −2.860 | 3.50 | 20.79 | 28.14 | 606.56 | 3 |
| R14 | −3.853 | 9.78 | 48.32 | 49.50 | 786.60 | 3 |
| R15 | −1.850 | 26.61 | 34.91 | 36.90 | 953.35 | 4 |
| R16 | −1.306 | 0.00 | 14.69 | 19.43 | 268.32 | 1 |
| R19 | −2.876 | 65.20 | 40.54 | 28.28 | 567.00 | 4 |

### *4.5. Exploratory Statistical Associations*

Cumulative gallery length within 50 m showed the strongest planimetric association with $|\Delta_Z|$ ($\rho = 0.734$, $p = 0.0008$, q = 0.010). Gallery length, extraction-sector coverage, and the number of distinct sectors remained positively associated at broader scales, including the 100–150 m annulus.

The association remained positive in all leave-one-benchmark-out iterations ($\rho = 0.674$–$0.804$; $p = 0.0002$–$0.0042$), indicating that it was not driven by a single benchmark. The additional resampling analyses supported the robustness of this association. The paired bootstrap produced a 95% confidence interval for Spearman's ρ of 0.388–0.924, while the two-sided Monte Carlo permutation test yielded $p = 0.0012$. Together with the leave-one-benchmark-out analysis, these results indicate that the observed association is not dependent on a single benchmark or on the asymptotic Spearman significance test alone.

The radius-sensitivity analysis showed that the positive association between cumulative principal-gallery length and $|\Delta_Z|$ was not restricted to the originally selected neighbourhood scales. Spearman coefficients were ρ = 0.380 ($p = 0.133$) at 25 m, ρ = 0.734 ($p = 0.0008$) at 50 m, ρ = 0.677 ($p = 0.0029$) at 75 m, ρ = 0.679 ($p = 0.0027$) at 100 m, ρ = 0.613 ($p = 0.0089$) at 125 m, and ρ = 0.648 ($p = 0.0049$) at 150 m. Thus, the association was weaker and not statistically supported at the very local 25 m scale, but remained consistently positive and statistically supported from 50 to 150 m. This sensitivity analysis supports the robustness of the observed relationship across intermediate neighbourhood scales while not identifying a unique or causal mining-influence radius.

Distance to the nearest principal gallery showed a moderate negative association ($\rho = -0.525$, $p = 0.0307$, q = 0.033), whereas distance to the nearest extraction sector was weaker and not statistically supported after adjustment ($\rho = -0.461$, $p = 0.0625$, q = 0.062).

The results therefore favour measures of surrounding mining concentration over nearest-sector distance alone. Because indicators were mutually correlated and benchmarks spatially clustered, the coefficients remain exploratory and do not identify a causal influence radius (Table 4; Figure 4).

**Table 4.** Exploratory Spearman rank correlations between the magnitude of the net 2007–2026 elevation difference, $|\Delta_Z|$, and selected planimetric mining indicators for the seventeen benchmarks. The q values represent Benjamini–Hochberg false-discovery-rate adjustments. The complete benchmark-level input dataset is provided in Supplementary Table S1.

| Mining Indicator | *n* | Spearman $\rho$ | *p* Value | q Value |
|---|---|---|---|---|
| Gallery length within 50 m | 17 | 0.734 | 0.0008 | 0.010 |
| Gallery length within 100 m | 17 | 0.679 | 0.0027 | 0.010 |
| Gallery length within 150 m | 17 | 0.648 | 0.0049 | 0.010 |
| Extraction-sector coverage within 50 m | 17 | 0.641 | 0.0056 | 0.010 |
| Extraction-sector coverage within 100 m | 17 | 0.642 | 0.0054 | 0.010 |
| Extraction-sector coverage within 150 m | 17 | 0.645 | 0.0052 | 0.010 |
| Distinct extraction sectors within 50 m | 17 | 0.661 | 0.0039 | 0.010 |
| Distinct extraction sectors within 150 m | 17 | 0.633 | 0.0064 | 0.010 |
| Gallery length within the 100–150 m annulus | 17 | 0.621 | 0.0078 | 0.011 |
| Extraction-sector coverage within the 100–150 m annulus | 17 | 0.616 | 0.0085 | 0.011 |
| Distance to nearest principal gallery | 17 | −0.525 | 0.0307 | 0.033 |
| Distance to nearest extraction sector | 17 | −0.461 | 0.0625 | 0.062 |
| Distinct extraction sectors within 100 m | 17 | 0.541 | 0.0250 | 0.029 |
| Distinct extraction sectors within the 100–150 m annulus | 17 | 0.633 | 0.0064 | 0.010 |

Note: The identical Spearman coefficients for "Distinct extraction sectors within 150 m" and "Distinct extraction sectors within the 100–150 m annulus" are not a transcription or duplication error. In the analysed dataset, the two benchmark-level count variables were identical for all seventeen benchmarks; consequently, their rank correlations with $|\Delta_Z|$ are also identical.

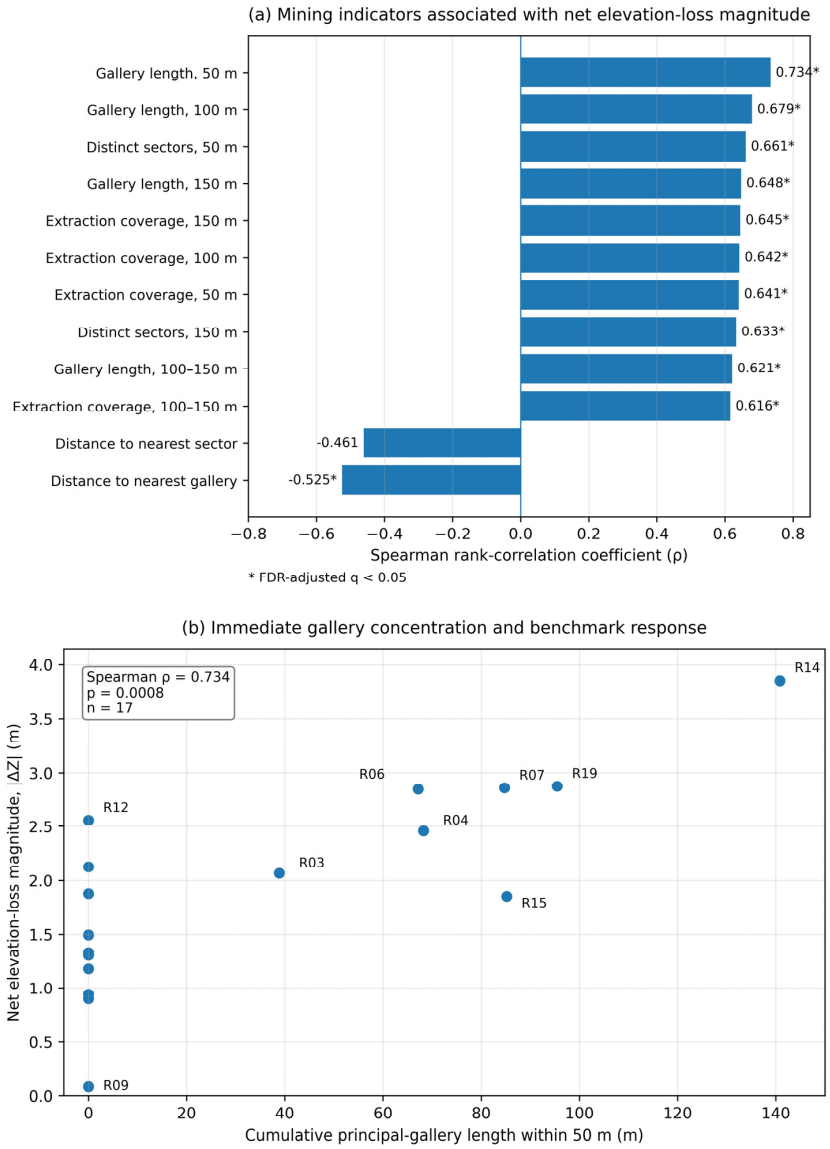



**Figure 4.** Exploratory relationships between the magnitude of the net 2007–2026 elevation difference, $|\Delta_Z|$, and the GIS-derived mining indicators: (**a**) Spearman rank-correlation coefficients for the selected planimetric variables, with asterisks indicating false-discovery-rate-adjusted q < 0.05; and (**b**) relationship between $|\Delta_Z|$ and cumulative principal-gallery length within 50 m of each benchmark. Benchmark labels identify representative and contrasting observations.

### *4.6. Exploratory Mining-Elevation Context*

Ten benchmarks had at least ten internally checked mining-elevation points within 150 m. R14 was surrounded by 28 points between 330.50 and 375.50 m and had a mean vertical separation of 454.02 m. Mean separations were 424.41 m at R19, 453.81 m at R07, 429.64 m at R06, and 248.73 m at R16.

The largest elevation losses were therefore not associated with the shallowest documented workings. $|\Delta_Z|$ was negatively associated with maximum, median, mean, and minimum mining elevation and positively associated with mean and minimum vertical separation. The strongest coefficient involved the standard deviation of mining elevations ($\rho = -0.952$, $p < 0.0001$, q < 0.001).

A leave-one-benchmark-out sensitivity analysis confirmed that the negative association remained consistently strong after sequential exclusion of each benchmark (Spearman $\rho = -0.933$ to $-0.983$), indicating that the result was not driven by any single observation.

Nevertheless, given the small sample size (n = 10) and the uneven spatial distribution of mining-elevation annotations, this relationship remains exploratory.

The relationship between the standard deviation of documented mining elevations within 150 m and the magnitude of net 2007–2026 elevation change is shown in Figure 5.

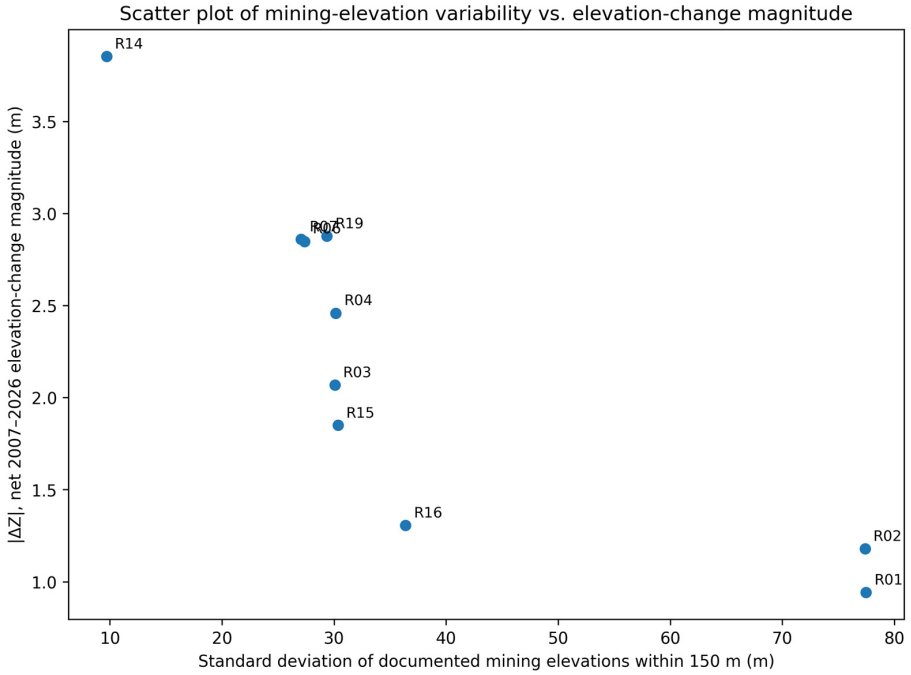



**Figure 5.** Relationship between the standard deviation of documented mining elevations within 150 m and the magnitude of net 2007–2026 elevation change, $|\Delta_Z|$, for the ten benchmarks with supported vertical information.

Given the small subset and the heterogeneous functional origin of the elevation annotations, these coefficients should be regarded as sensitivity indicators rather than as evidence of an independent vertical control on the observed net elevation change.

This result is sensitive to the uneven number, distribution, and functional type of the annotations. Associations involving the number of internally checked mining-elevation points and the total documented elevation range were not statistically supported after adjustment. These vertical indicators describe the surrounding documented mining context; they do not represent exact panel depths beneath individual benchmarks or establish an independent depth-control mechanism (Table 5).

**Table 5.** Exploratory sensitivity analysis based on Spearman rank correlations between the magnitude of the net 2007–2026 elevation difference, $|\Delta_Z|$, and mining-elevation indicators for the ten benchmarks with at least ten internally checked mining-elevation points within 150 m. The q values represent Benjamini–Hochberg false-discovery-rate adjustments.

| Mining-Elevation Indicator | n | Spearman $\rho$ | $p$ Value | q Value |
|---|---|---|---|---|
| Standard deviation of documented mining elevations | 10 | −0.952 | <0.0001 | <0.001 |
| Maximum documented mining elevation | 10 | −0.899 | 0.0004 | 0.002 |
| Median documented mining elevation | 10 | −0.851 | 0.0018 | 0.006 |
| Mean documented mining elevation | 10 | −0.842 | 0.0022 | 0.006 |
| Minimum documented mining elevation | 10 | −0.787 | 0.0069 | 0.013 |
| Mean vertical separation | 10 | 0.782 | 0.0075 | 0.013 |
| Minimum vertical separation | 10 | 0.721 | 0.0186 | 0.027 |
| Maximum vertical separation | 10 | 0.648 | 0.0425 | 0.053 |
| Number of internally checked mining-elevation points | 10 | 0.588 | 0.0739 | 0.082 |
| Documented elevation range | 10 | −0.445 | 0.1974 | 0.197 |

Nevertheless, because only ten benchmarks were included and the mining-elevation annotations were unevenly distributed, this relationship remains exploratory and should not be interpreted as evidence of an independent depth-control mechanism.

## 5. Discussion

### *5.1. Cumulative Mining Configuration Versus Nearest-Feature Interpretation*

The main finding is that spatially variable elevation loss was more consistently associated with the cumulative configuration of panels and galleries than with nearest-sector distance alone. This is geologically and operationally plausible in a sector developed through adjoining extraction areas, interconnected infrastructure, and successive mining stages.

The contrasting benchmarks illustrate this point. R19 was dominated by immediate sector exposure, R14 by a broader surrounding concentration, and R06–R07 by mixed proximity to galleries and several sectors. R15 had the greatest 150 m gallery length without the greatest loss, whereas R12 provides an important counter-example to a simple mining-proximity interpretation. Despite its relatively large net elevation loss (−2.556 m), no reconstructed mining feature occurs within more than 600 m of the benchmark. This discrepancy may indicate incomplete archival representation of the underground workings or the contribution of geological, hydrogeological, benchmark-specific, or other non-mining factors that were not quantified in the present study. R12 therefore reinforces the interpretation that the GIS-derived exposure indicators describe spatial associations rather than a complete or causal explanation of the observed elevation changes. Thus, containment, distance, coverage, or gallery length should not be interpreted independently.

The strong association for gallery length within 50 m does not define a mechanical influence radius. Overlapping neighbourhoods, correlated indicators, spatial clustering, incomplete archival coverage, and unmeasured geological factors preclude causal attribution to an individual panel or gallery.

### *5.2. Significance of the Reconstructed Mining Chronology*

The reconstructed 2000–2007 sequence shows that later extraction occurred in a rock mass already modified by earlier workings. Successive caving, fracturing, stress redistribution, and compaction may therefore have produced cumulative effects [1–7].

Recent numerical studies of repeated and multi-slice coal extraction similarly show that successive mining stages can modify stress redistribution, fracture development, overburden movement, and the magnitude of surface subsidence [21,22]. These findings support interpreting the reconstructed Maleia–Livezeni workings as a cumulative mining configuration, although the present two-epoch dataset does not permit temporal attribution of individual surface movements to specific extraction stages.

An important temporal limitation is that the reconstructed mining chronology mainly represents workings developed during 2000–2007, whereas the surface response is represented only by the net elevation difference between 2007 and 2026. Consequently, the spatial associations identified in this study cannot determine whether the observed elevation losses occurred shortly after mining, accumulated progressively during the nineteen-year interval, or resulted from later episodic deformation. The reconstructed chronology therefore supports interpretation of cumulative historical mining exposure, but it cannot be used to establish a temporal cause-and-effect relationship between individual mining stages and the measured surface response.

### *5.3. Geological Context and Geomechanical Interpretation*

Coal Seam No. 3 occurs within alternating competent sandstones and weaker claystones, marls, and carbonaceous shales. Following roof caving, these contrasts may influence bridging, fracture development, stress transfer, and delayed compaction; successive extraction may enlarge the disturbed rock volume [1–7].

In another sector of the Jiu Valley, discontinuous post-mining deformation was associated with the combined influence of thick-seam extraction, longwall top-coal caving, relatively shallow workings, and nearby faults [23]. Although the mining and geological conditions are not identical to those at Maleia–Livezeni, this case illustrates the importance of considering mining geometry together with structural controls.

The observed patterns are compatible with these mechanisms but do not quantify them. Mining depth, extracted thickness, seam inclination, faults, groundwater, and rock-mass properties were not available uniformly at benchmark scale. The 567 internally checked mining-elevation annotations add partial vertical context but represent different mining features rather than complete panel geometry.

Recent numerical work on soft–hard interbedded rock masses further indicates that contrasts in mechanical properties and layer inclination can influence crack initiation, propagation, strength, and failure mode [24]. Although that study was not conducted in a mining-subsidence setting, it provides additional support for treating lithological heterogeneity as a potentially important control that cannot be quantified with the present benchmark-scale dataset.

Geology therefore provides an interpretative framework, not proof of a unique mechanism. Panel-specific three-dimensional geometry, boreholes, structural and hydrogeological observations, and rock-mechanical parameters would be required for causal assessment.

### *5.4. Contribution and Practical Implications*

Relative to previous deformation-monitoring studies and GIS reconstructions of legacy mine information, the contribution of the present study lies in the integrated workflow rather than in any single dataset. The workflow reconstructs extraction-sector geometry and chronology, derives benchmark-level mining-exposure indicators at multiple spatial scales, incorporates internally checked underground-elevation annotations, and evaluates these variables against the available net 2007–2026 benchmark elevation changes. This integration extends archival mine-plan reconstruction from documentation and inventory toward an exploratory spatial framework for interpreting heterogeneous surface response. The workflow can support first-level screening in former mining districts where archival documentation survives but complete three-dimensional models do not. Locations surrounded by several sectors or dense gallery networks can be prioritised for renewed GNSS or interferometric synthetic aperture radar (InSAR) monitoring and site-specific geological or geotechnical investigation.

The indicators are screening variables only. The 50, 100, and 150 m radii are analytical scales, and high exposure does not establish present instability, a legal hazard zone, or a geotechnical safety boundary.

### *5.5. Limitations and Future Research*

The main limitations arise from the heterogeneous scale, quality, completeness, and positional accuracy of the archival plans. Reconstructed features are plan-based estimates, and the two-dimensional buffers do not incorporate complete depth, seam inclination, extracted thickness, or disturbed-rock geometry. Overlapping neighbourhoods also reduce statistical independence.

The temporal resolution is also limited. Mining chronology is documented mainly for 2000–2007, whereas surface elevation is available only for the 2007 and 2026 observation epochs. This mismatch prevents reconstruction of the temporal evolution of the measured elevation changes and precludes attribution of specific surface responses to individual mining stages. The network contains seventeen spatially clustered benchmarks, and the vertical analysis includes ten. The 567 internally checked mining-elevation annotations are unevenly distributed and do not form a complete three-dimensional mine model. Benchmark-scale lithological, structural, hydrogeological, and rock-mechanical data were unavailable.

Future work should add GNSS or InSAR epochs, denser monitoring, panel-specific depth and extraction data, borehole and fault information, groundwater observations, and calibrated three-dimensional geomechanical modelling.

This recommendation is consistent with recent reviews emphasizing the complementary roles of GNSS, InSAR, numerical modelling, and multi-source monitoring for assessing mining-induced ground deformation in complex geological settings [25].

The R12 observation illustrates this limitation directly: a substantial net elevation loss occurs at a benchmark for which the available archival reconstruction indicates no nearby mining exposure, demonstrating that the reconstructed geometry cannot account for all observed surface-elevation changes.

Although leave-one-out, bootstrap, and permutation analyses were used to evaluate the robustness of the principal association, these procedures do not account explicitly for spatial dependence among the clustered benchmarks or overlapping exposure neighbourhoods. The statistical results therefore remain exploratory.

## 6. Conclusions

This study reconstructed twelve extraction sectors, principal galleries, mining stages, and 567 internally checked mining-elevation annotations for Coal Seam No. 3 in the Maleia–Livezeni sector and integrated them with net 2007–2026 elevation differences at seventeen benchmarks.

Mining-feature concentration was more consistently associated with elevation-loss magnitude than nearest-sector distance alone. Gallery length within 50 m showed the strongest planimetric association, while sector coverage, gallery length, and the number of surrounding sectors remained informative at broader scales. The contrasting configurations of R19, R14, R06, R07, and R15 show that no individual GIS indicator explains the complete response.

The mining-elevation data provided partial vertical context but did not show that the largest losses occurred above the shallowest workings. Because the archival geometry is incomplete, the sample is small and spatially clustered, and benchmark-scale geological data are unavailable, the results are exploratory rather than causal.

The workflow is useful for preliminary screening in former underground-mining areas and for prioritising additional monitoring, but its buffer radii are comparative GIS scales, not calibrated influence or hazard limits. Denser deformation observations and three-dimensional geological and mine models are required for predictive assessment.

The positive association between cumulative gallery length and net elevation-change magnitude remained consistent across the additional 25–150 m radius-sensitivity analysis, supporting the robustness of the multi-scale interpretation.

**Supplementary Materials:** The following supporting information can be downloaded at: https://www.mdpi.com/article/10.3390/mining6030079/s1, Table S1. Complete benchmark-level dataset used in the exploratory planimetric and vertical analyses. Table S2. Benchmark-level cumulative principal-gallery lengths used in the radius-sensitivity analysis at 25, 50, 75, 100, 125, and 150 m.

File S1. Python script used to reproduce the Spearman correlation analyses, Benjamini–Hochberg false-discovery-rate adjustments, leave-one-benchmark-out sensitivity analyses, bootstrap confidence interval, permutation test, radius-sensitivity analysis, and vertical scatter plot.

**Author Contributions:** Conceptualization, T.G. and V.P.; methodology, T.G. and V.P.; software, T.G.; formal analysis, T.G.; investigation, T.G.; data curation, T.G.; visualization, T.G.; writing—original draft preparation, T.G.; writing—review and editing, T.G. and V.P.; validation, V.P. All authors have read and agreed to the published version of the manuscript.

**Funding:** This research received no external funding.

**Institutional Review Board Statement:** Not applicable.

**Informed Consent Statement:** Not applicable.

**Data Availability Statement:** The 2007–2026 GNSS elevation-difference dataset is reported in reference [17]. The complete benchmark-level dataset used in the present planimetric and vertical analyses is provided in Supplementary Table S1, and the benchmark-level cumulative principal-gallery lengths used in the radius-sensitivity analysis are provided in Supplementary Table S2. The statistical calculations, including the Spearman correlations, Benjamini–Hochberg adjustments, leave-one-benchmark-out analyses, bootstrap confidence interval, permutation test, and radius-sensitivity analysis, can be reproduced using the Python script provided as Supplementary File S1. The archival mine plans and coordinate-referenced DXF compilation contain historical mining information subject to institutional and archival restrictions and are therefore not included in the public Supplementary Materials. Derived GIS layers may be made available for scientific verification where permitted by the applicable institutional and archival restrictions.

**Acknowledgments:** The authors acknowledge the historical CEEX project documentation and archived mining plans that supported reconstruction of the underground mining geometry in the Maleia–Livezeni sector.

**Conflicts of Interest:** The authors declare no conflicts of interest.

## References

1. Peng, S.S. *Surface Subsidence Engineering*; Society for Mining, Metallurgy and Exploration: Littleton, CO, USA, 1992.
2. Whittaker, B.N.; Reddish, D.J. *Subsidence: Occurrence, Prediction and Control*; Elsevier: Amsterdam, The Netherlands, 1989.
3. Kratzsch, H. *Mining Subsidence Engineering*; Springer: Berlin/Heidelberg, Germany, 1983. [CrossRef]
4. Bell, F.G.; Stacey, T.R.; Genske, D.D. Mining Subsidence and Its Effect on the Environment: Some Differing Examples. *Environ. Geol.* **2000**, *40*, 135–152. [CrossRef]
5. Singh, R.P.; Dhar, B.B. Influence of Mine Geometry on Surface Subsidence Prediction. *Int. J. Rock Mech. Min. Sci.* **1997**, *34*, 1147–1158.
6. Brady, B.H.G.; Brown, E.T. *Rock Mechanics for Underground Mining*, 3rd ed.; Springer: Dordrecht, The Netherlands, 2004. [CrossRef]
7. Strozik, G.; Jendruś, R.; Manowska, A.; Popczyk, M. Mine Subsidence as a Post-Mining Effect in the Upper Silesia Coal Basin. *Pol. J. Environ. Stud.* **2016**, *25*, 777–785. [CrossRef]
8. Blachowski, J.; Ellefmo, S.L. Mining Ground Deformation Estimation Based on Pre-Processed InSAR Open Data—A Norwegian Case Study. *Minerals* **2023**, *13*, 328. [CrossRef]
9. Cai, Y.; Jin, Y.; Wang, Z.; Chen, T.; Wang, Y.; Kong, W.; Xiao, W.; Li, X.; Lian, X.; Hu, H. A Review of Monitoring, Calculation, and Simulation Methods for Ground Subsidence Induced by Coal Mining. *Int. J. Coal Sci. Technol.* **2023**, *10*, 32. [CrossRef]
10. Lian, X.; Shi, L.; Kong, W.; Han, Y.; Fan, H. Residual Subsidence Time Series Model in Mountain Area Caused by Underground Mining Based on GNSS Online Monitoring. *Int. J. Coal Sci. Technol.* **2024**, *11*, 27. [CrossRef]
11. Ma, Z.; Yang, X.; Xie, L.; Dong, W. Life Cycle Mining Deformation Monitoring and Analysis Using Sentinel-1 and Radarsat-2 InSAR Time Series. *Remote Sens.* **2024**, *16*, 2335. [CrossRef]
12. Hvizdák, L.; Tometzová, D.; Iannaccone, B.; Šoltésová, M.; Domaracká, L.; Kyšeľa, K. Old Mine Map Georeferencing: Case of Marsigli's 1696 Map of the Smolník Mines. *ISPRS Int. J. Geo-Inf.* **2023**, *12*, 345. [CrossRef]
13. Bindzarova Gergelova, M.; Labant, S.; Mizak, J.; Sustek, P.; Leicher, L. Inventory of Locations of Old Mining Works Using LiDAR Data: A Case Study in Slovakia. *Sustainability* **2021**, *13*, 6981. [CrossRef]
14. Muntean, A.; Mocanu, V.; Ambrosius, B. A GPS Study of Land Subsidence in the Petroșani (Romania) Coal Mining Area. *Nat. Hazards* **2016**, *80*, 797–810. [CrossRef]

15. University of Bucharest; National Institute for Earth Physics; University of Petroșani. *Subsidence of Lands Affected by Underground Mining: The Case of the Petroșani Mining Basin; CEEX Programme*; Contract No. 722/2006, Research and Scientific–Technical Reports, Stages I–IV; University of Bucharest: Bucharest, Romania, 2008. (In Romanian)
16. Belkin, H.E.; Tewalt, S.J.; Hower, J.C.; Stucker, J.D.; O'Keefe, J.M.K.; Tatu, C.A.; Buia, G. Petrography and Geochemistry of Oligocene Bituminous Coal from the Jiu Valley, Petroșani Basin (Southern Carpathian Mountains), Romania. *Int. J. Coal Geol.* **2010**, *82*, 68–80. [CrossRef]
17. Gavrilescu, T.; Păunescu, C. Persistent Mining-Induced Subsidence Two Decades after Underground Coal Exploitation: Evidence from Multi-Temporal GNSS Monitoring. *Mining* **2026**, *6*, 57. [CrossRef]
18. Graser, A.; Sutton, T.; Bernasocchi, M. The QGIS Project: Spatial without Compromise. *Patterns* **2025**, *6*, 101265. [CrossRef]
19. Benjamini, Y.; Hochberg, Y. Controlling the False Discovery Rate: A Practical and Powerful Approach to Multiple Testing. *J. R. Stat. Soc. Ser. B* **1995**, *57*, 289–300. [CrossRef]
20. Virtanen, P.; Gommers, R.; Oliphant, T.E.; Haberland, M.; Reddy, T.; Cournapeau, D.; Burovski, E.; Peterson, P.; Weckesser, W.; Bright, J.; et al. SciPy 1.0: Fundamental Algorithms for Scientific Computing in Python. *Nat. Methods* **2020**, *17*, 261–272. [CrossRef]
21. Peng, N.; Zhang, C.; Feng, R.; Arif, A.; Chen, X.; Zhang, W.; Zhang, S.; Feng, M. Analysis of Dynamic Evolution of Surrounding Rock Movement and Stress-Fracture in the Upward and Repeated Mining of Close-Distance Coal Seams. *Adv. Civ. Eng.* **2024**, *2024*, 5548837. [CrossRef]
22. Zhang, C.; Arif, A.; Wu, J.; Habibullah, M.; Mohammadamini, K.; Sajib, M.H.; Manohar, B. Investigation of Surface Subsidence Behaviour in Multi-Slice Longwall Mining Using Numerical Simulations in Barapukuria Coal Mine, Bangladesh. *Sci. Rep.* **2026**, *16*, 422. [CrossRef]
23. Marian, D.P.; Onica, I. Analysis of the Geomechanical Phenomena That Led to the Appearance of Sinkholes at the Lupeni Mine, Romania, in the Conditions of Thick Coal Seams Mining with Longwall Top Coal Caving. *Sustainability* **2021**, *13*, 6449. [CrossRef]
24. Zhang, C.; Feng, M.; Feng, R.; Arif, A.; Peng, N.; Zhuang, W.; Zhong, Y. Numerical Studies of Soft and Hard Interbedded Rock Mass Failures with Different Laying Inclinations. *Bull. Eng. Geol. Environ.* **2026**, *85*, 315. [CrossRef]
25. Arif, A.; Zhang, C.; Feng, M.; Sajib, M.H.; Habibullah, M.; Hasan, S.; Rana, M.S.; Mohammadamini, K.; Alip, M.; Zhang, Y. Mining-Induced Subsidence Predicting and Monitoring: A Comprehensive Review of Methods and Technologies. *Geotech. Geol. Eng.* **2025**, *43*, 314. [CrossRef]

**Disclaimer/Publisher's Note:** The statements, opinions and data contained in all publications are solely those of the individual author(s) and contributor(s) and not of MDPI and/or the editor(s). MDPI and/or the editor(s) disclaim responsibility for any injury to people or property resulting from any ideas, methods, instructions or products referred to in the content.